Eur. Phys. J. C (2016) 76:482
DOI 10.1140/epjc/s10052-016-4330-3

THE EUROPEAN PHYSICAL JOURNAL C

Regular Article - Theoretical Physics

Prompt signals and displaced vertices in sparticle searches for next-to-minimal gauge-mediated supersymmetric models

B. C. Allanach[1,a], **Marcin Badziak**[2,3,4,b], **Giovanna Cottin**[5,c], **Nishita Desai**[6,d], **Cyril Hugonie**[7,e], **Robert Ziegler**[8,9,f]

[1] Department of Applied Mathematics and Theoretical Physics, Centre for Mathematical Sciences, University of Cambridge, Wilberforce Road, Cambridge CB3 0WA, UK
[2] Institute of Theoretical Physics, Faculty of Physics, University of Warsaw, ul. Pasteura 5, 02-093 Warsaw, Poland
[3] Department of Physics, University of California, Berkeley, CA 94720, USA
[4] Ernest Orlando Lawrence Berkeley National Laboratory, University of California, Berkeley, CA 94720, USA
[5] Cavendish Laboratory, University of Cambridge, 19 JJ Thomson Ave, Cambridge CB3 0HW, UK
[6] Institut für Theoretische Physik, Philosophenweg 16, 69120 Heidelberg, Germany
[7] LUPM, UMR 5299, CNRS, Université de Montpellier, 34095 Montpellier, France
[8] Sorbonne Universités, UPMC Univ Paris 06, UMR 7589, LPTHE, 75005 Paris, France
[9] CNRS, UMR 7589, LPTHE, 75005 Paris, France

Received: 27 June 2016 / Accepted: 19 August 2016 / Published online: 1 September 2016

Abstract We study the LHC phenomenology of the next-to-minimal model of gauge-mediated supersymmetry breaking, both for Run I and Run II. The Higgs phenomenology of the model is consistent with observations: a 125 GeV standard model-like Higgs which mixes with singlet-like state of mass around 90 GeV that provides a 2σ excess at LEP II. The model possesses regions of parameter space where a longer-lived lightest neutralino decays in the detector into a gravitino and a b-jet pair or a tau pair resulting in potential displaced vertex signatures. We investigate current bounds on sparticle masses and the discovery potential of the model, both via conventional searches and via searches for displaced vertices. The searches based on promptly decaying sparticles currently give a lower limit on the gluino mass 1080 GeV and could be sensitive up to 1900 GeV with 100 fb^{-1}, whereas the current displaced vertex searches cannot probe this model due to b-quarks in the final state. We show how the displaced vertex cuts might be relaxed in order to improve signal efficiency, while simultaneously applied prompt cuts reduce background, resulting in a much better sensitivity than either strategy alone and motivating a fully fledged experimental study.

[a] e-mail: b.c.allanach@damtp.cam.ac.uk
[b] e-mail: mbadziak@fuw.edu.pl
[c] e-mail: gfc24@cam.ac.uk
[d] e-mail: n.desai@thphys.uni-heidelberg.de
[e] e-mail: cyril.hugonie@umontpellier.fr
[f] e-mail: robert.ziegler@lpthe.jussieu.fr

1 Introduction

Sparticle searches at the large hadron collider (LHC) have so far yielded no clear discovery. Strengthening exclusion limits [1] on the masses of sparticles in the minimal supersymmetric standard model (MSSM) mean that points in the model parameter space with low fine-tuning have been ruled out. In particular, the ATLAS and CMS experiments have measured a particle whose properties are compatible with a standard model (SM) Higgs of mass around 125 GeV. While such a mass is still compatible with the theoretical upper bound in the MSSM, it is rather on the heavy side and corresponds to a fairly heavy stop mass, which in turn induces lower bounds on typical quantifications of fine-tuning in the electroweak symmetry breaking sector (see e.g. Ref. [2]). Arguably, it may be important to consider non-minimal supersymmetric scenarios that can alter the interpretation of standard sparticle searches, perhaps allowing regions with lower fine-tuning than in minimal scenarios. However, one may get an impression from "simplified model searches" (where the MSSM spectrum is set to be heavy except for a few sparticles relevant for a particular search) that strongly interacting particles with multi-TeV masses are already ruled out (see, for example Ref. [1]), eliminating the low fine-tuning regions. Still, in more realistic non-simplified MSSM scenarios, points in parameter space exist with gluino masses of 700 GeV or squark masses of 500 GeV which evade all Run I sparticle searches [3] or even which evade all 2015 Run II searches [4] with consequently fairly low values of fine-tuning.

Non-simplified MSSM scenarios are suggested by well motivated ultra-violet scenarios of SUSY breaking, for example Gauge Mediation. While gauge-mediated SUSY breaking provides a neat solution to the SUSY flavour problem (i.e. the absence of large sources of flavour violation in the soft terms), its minimal realisations are in trouble because they typically predict a SM-like Higgs mass that is too low compared to the observed value around 125 GeV. A potentially fruitful path was explored by introducing additional dynamics to increase the SM-like Higgs boson mass prediction while maintaining fairly low levels of fine-tuning, see Refs. [5–25].

In Ref. [26], we revisited a simple model by Delgado et al. [27] (DGS) that combines gauge mediation (GM) and the next-to-minimal supersymmetric standard model (NMSSM). The field content of the model is the one of the NMSSM, plus two copies of messengers in $\mathbf{5}+\bar{\mathbf{5}}$ representations of SU(5), denoted by $\Phi_i, \bar{\Phi}_i$, respectively ($i \in \{1, 2\}$), with doublet and triplet components $\Phi_i^D, \bar{\Phi}_i^D$ and $\Phi_i^T, \bar{\Phi}_i^T$. SUSY breaking is parameterised by the spurion $X = M + F\theta^2$ (where M is the messenger scale and θ is the Grassmann valued $N = 1$ superspace coordinate). Aside from Yukawa interactions, the superpotential contains spurion–messenger couplings and singlet S–messenger couplings (first introduced in the context of gauge mediation in Ref. [28]):

$$\begin{aligned} W = \cdots &+ \lambda S H_u H_d + \frac{\kappa}{3} S^3 \\ &+ X \sum_i (\kappa_i^D \bar{\Phi}_i^D \Phi_i^D + \kappa_i^T \bar{\Phi}_i^T \bar{\Phi}_i^T) \\ &+ S(\xi_D \bar{\Phi}_1^D \Phi_2^D + \xi_T \bar{\Phi}_1^T \Phi_2^T), \end{aligned} \tag{1}$$

where the singlet–messenger couplings unify at the grand unified theory scale M_{GUT}: $\xi_D(M_{\mathrm{GUT}}) = \xi_T(M_{\mathrm{GUT}}) \equiv \xi$ with unified coupling ξ. The scale of the SUSY breaking terms is fixed by the parameter $\tilde{m} = 1/(16\pi^2)F/M$.

It was shown in Ref. [26] that in the DGS model one can obtain a 125 GeV standard model-like Higgs boson with stops as light as 1.1 TeV, thanks to the mixing of the Higgs with a singlet state at $\mathcal{O}(90-100)$ GeV which is compatible with LEP data [29]. With these Higgs constraints, essentially all parameters are fixed except for the GM messenger scale which mainly controls the phenomenology of the gravitino. The central feature of the model, apart from the light Higgs that might explain the LEP excess [30] is the peculiar structure of the light sparticle spectrum. The lightest sparticle (LSP) is the gravitino[1] $\tilde{G}$ with mass and couplings effectively set by the GM messenger scale, the next-to-LSP (NLSP) is a singlino-like neutralino $\tilde{N}_1$ of mass around 100 GeV, and the next-to-NLSP (NNLSP) is a bino-like neutralino $\tilde{N}_2$ or stau $\tilde{\tau}$, depending on the GM messenger scale. The presence of the singlino alters SUSY decay chains as compared to the MSSM, leading to additional b-jets or taus. One distinctive feature of this scenario is that the singlino decays to a gravitino and a light singlet-like pseudo-scalar a_1 of mass around 20 GeV, with the latter decaying predominantly to $b\bar{b}$ as well as to $\tau\tau$. Depending on the GM messenger scale, the two b-jets may be produced far outside the detector (when the $\tilde{N}_1$ is quasi-stable, at high GM scales) or at low GM scales, they may be produced within the detector from displaced vertices (DVs). This peculiar feature of a long-lived singlino decay was already noticed in Ref. [27]. An example diagram showing LHC sparticle production in the model is shown in Fig. 1.

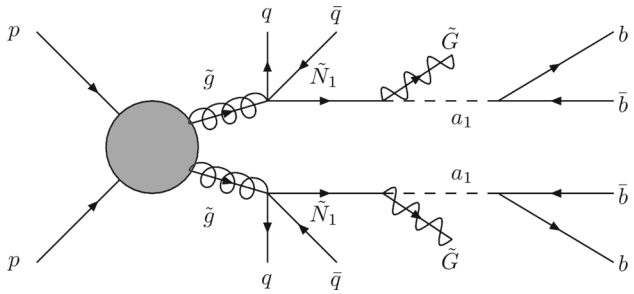

Fig. 1 An example of LHC sparticle production in the DGS model, followed by sparticle decay. In this example, we have four hard prompt jets from gluinos decaying into quarks q and anti-quarks $\bar{q}$; the lightest neutralino $\tilde{N}_1$ may have an intermediate lifetime, producing displaced vertices, each generating $b\bar{b}$. The gravitino $\tilde{G}$ leaves a missing transverse momentum signature. The lightest pseudo-scalar a_1 has a lower branching ratio for decays into $\tau\bar{\tau}$ than $b\bar{b}$. The $\tilde{g} \to \tilde{N}_1$ part of the decay may commonly be more complicated, involving a cascade decay and concomitant additional SM states

In this paper, we wish to evaluate the collider phenomenology of the model. In Sect. 2, we describe our benchmark model, and describe the tools used for simulation of the signal events and validation of our analysis. In Sect. 3, we recast the most constraining prompt sparticle searches from the LHC in order to find how stringent the bounds on the model are and then we estimate the future reach. In Sect. 4, we detail a study of DV signatures, starting with recasting the current ATLAS multi-track DV + jets analysis and showing that current searches are not sensitive to our model. By changing the cuts, we suggest ways in which the DV cuts can be loosened, and how cuts on accompanying hard prompt objects can be used to combat background rates. In Sect. 4.4, we estimate the search reach from early Run II data with such a strategy. After a summary and discussion in Sect. 5, we define the relevant DV variables d_0 and r_{DV} in Appendix A, for easy reference by the reader.

[1] Another attractive feature of the NMSSM realisation of gauge mediation is that the singlet allows the gravitino to be a good dark matter candidate even for large reheating temperatures that are compatible with thermal leptogenesis [31].

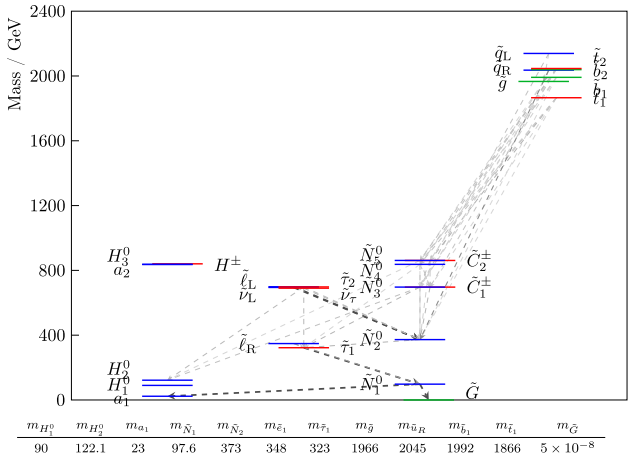

Fig. 2 Spectrum and the more likely sparticle decays of benchmark point P0: $\xi = 0.01$, $\lambda(M_{\rm SUSY}) = 0.009$, $M = 1.4 \times 10^6$ GeV, $\tilde{m} = 863$ GeV and $\tan\beta = 28.8$. Decays into sparticles which have a branching ratio greater than 10 % are displayed by the *arrows*. The figure was produced with the help of `PySLHA3.0.4` [34]. The *table* shows some more precise details of the spectrum of the benchmark point P0. All masses are listed in GeV units and the lightest neutralino has a decay length $c\tau_{\tilde{N}_1} = 99$ mm

2 Benchmark model and event generation

Here, we discuss the limits from the LHC, both in prompt and displaced searches. Like minimal gauge mediation in the MSSM, the DGS model also needs large radiative SUSY corrections to obtain the correct Higgs mass (although the singlet–Higgs mixing helps). In order to be concrete, we choose to study a benchmark point P0, whose spectrum (as generated by NMSSMTOOLS 4.9.2 [32,33]) is shown in Fig. 2. P0 has a SM-like Higgs in the vicinity of the measured mass at 125 GeV (allowing for a 3 GeV theoretical uncertainty in its prediction) and a lighter CP-even Higgs at 90 GeV that couples with a reduced strength (compared to a SM Higgs) to Z-bosons, commensurate with a 2σ LEP excess. In addition, the lightest singlet-like pseudo-scalar a_1 has a mass of 23 GeV and the singlino-like NLSP $\tilde{N}_1$ has a mass of 98 GeV.

We generate event samples with PYTHIA 8.2 [35], using FASTJET 3.1.3 [36] for jet reconstruction. The ATLAS models we wish to validate, described in Sect. 4.1, are generated with SOFTSUSY 3.6.1 [37,38] to calculate the spectra and SDECAY 1.5 [39] to generate the decays, communicating the spectrum and decay information via SUSY Les Houches Accord (SLHA) files [40,41].

To take into account the size of the detector, we consider a cylinder with radius $r = 11$ m and length $|z| = 28$ m, corresponding to the ATLAS inner detector [42]. It is possible for a neutral particle that decays outside the inner detector to form trackless jets. However, it is difficult to model the detector response to these and so we consider them to be beyond the scope of this study. Any particle that decays outside the inner detector is therefore considered to be stable for all intents and purposes. The detector response for measurement of jet p_T is modelled as follows.[2] The jet momentum is smeared by a gaussian with resolution of 20 % of energy for $E_{\rm jet} < 50$ GeV, falling linearly to 10 % up to 100 GeV and then a flat 10 %. A further scale correction of 1 % is applied for jets with $|\eta| < 2$ and 3 % for those with higher $|\eta|$.

With this parameterisation, we are able reproduce the cut flows for the ATLAS 0-lepton + jets + missing transverse energy[3] ($p_T^{\rm miss}$) analyses and the efficiencies are validated against published results for benchmarks provided in the ATLAS analysis documentation. Further fiducial and material cuts required for tracks in the DV studies are explained in Sect. 4.1.

3 Prompt SUSY searches

In order to determine constraints on the gluino mass in our model, we focus on the 0-lepton + two–six jets + $p_T^{\rm miss}$ search [43,44] which is the most sensitive search for benchmark P0. However, to investigate the response of our model to dedicated SUSY searches, we deform it by moving on a line into the phenomenological next-to-minimal model space (pNMSSM): for instance, we vary the gluino mass soft parameter M_3 while keeping all other weak-scale parameters fixed. The spectrum, decays and lifetimes are recomputed at each point: to first order, only the gluino mass changes, but there are small loop-level effects on other masses. Since this deformation breaks the gauge-mediated relation between the gaugino masses, we are deviating from the gauge-mediated limit by doing this. This is a simple choice where we can change only one parameter; we could have equally made a different choice where we vary several weak-scale parameters—trying to preserve some of the gauge-mediated relations. Keeping within the NMGMSB model itself was not an option however, since a highly non-trivial multi-dimensional manipulation of parameters was required, which ended in some other phenomenological bound being violated. Our approach is mainly phenomenologically motivated, essentially to study the gluino mass bounds in the context of the very peculiar structure of singlino-like NLSP and gravitino LSP (with squarks decoupled). Nevertheless one might imagine a possible extension of the DGS scenario with additional sources for the Higgs

[2] We find inconsistent results from standard detector simulation programs leading us to believe that the presence of DVs interferes with the standard reconstruction.

[3] We prefer to use the more accurate descriptor $p_T^{\rm miss} = |\mathbf{p}_T^{\rm miss}|$ than the '$E_T^{\rm miss}$' quoted by the ATLAS analyses referred to in this study.

Table 1 The cuts for more sensitive signal regions from the 0-lepton + jets + p_T^{miss} searches at 8 TeV [43] and 13 TeV [44] runs and 95 % observed upper limits on a non-standard model contribution σ_{95}^{obs}. The limit σ_{95}^{obs} has not been unfolded, and so should be applied to the production cross section times branching ratio times acceptance. The jets j are ordered in decreasing p_T. The effective mass, m_{eff}(incl.) is defined to be the scalar sum of p_T's of all jets with $p_T > 40(50)$ GeV for $\sqrt{s}$ =8 (13) TeV plus the missing transverse momentum p_T^{miss}, $m_{\text{eff}}(N_j)$ is the scalar sum of p_T's of N_j hardest jets ($N_j = 4$ for `4jt-X` and $N_j = 6$ for `6jt-X`) plus p_T^{miss} and ϕ is the azimuthal angle around the beam

$\sqrt{s}$	8 TeV		13 TeV	
Signal region	`4jt-8`	`6jt-8`	`4jt-13`	`6jt-13`
p_T^{miss}/GeV >	160	160	200	200
$p_T(j_1)$/GeV >	130	130	200	200
$p_T(j_2)$/GeV >	60	60	100	100
$p_T(j_3)$/GeV >	60	60	100	100
$p_T(j_4)$/GeV >	60	60	100	100
$p_T(j_5)$/GeV >	–	60	–	50
$p_T(j_6)$/GeV >	–	60	–	50
$\Delta\phi(\text{jet}_{1,2,3}, \mathbf{p}_T^{\text{miss}})_{\text{min}}$ >	0.4			
$\Delta\phi(\text{jet}_{j>3}, \mathbf{p}_T^{\text{miss}})_{\text{min}}$ >	0.2			
$p_T^{\text{miss}}/m_{\text{eff}}(N_j)$ >	0.25		0.2	
m_{eff}(incl.)/GeV >	2200	1500	2200	2000
σ_{95}^{obs} (fb)	0.15	0.32	2.7	1.6

mass that allow one to lower the overall scale of sparticle masses to the investigated range.

We have also sometimes, for the purposes of illustration only, changed the singlino decay length $c\tau_{\tilde{N}_1}$ (while keeping all weak-scale parameters fixed). This deformation does not really constitute a consistent model, but is used instead to understand some features that are present in consistent models. When using this type of deformation we will refer to 'tweaked' parameters. We shall investigate the effect of varying the lifetime by scanning over a lifetime range of $c\tau = [10^{-3},\ 10^{4}]$ mm for $m_{\tilde{g}} \sim 1$ TeV.

3.1 Current bounds from Run I and early Run II searches

In the NMGMSB model under study, the squarks (including the third generation squarks) are usually heavier than the gluino, resulting in three-body decays through off-shell squarks of the form $\tilde{g} \to q\bar{q}\tilde{N}_1$, where $\tilde{N}_1$ is mostly singlino-like, followed by the potentially displaced decay $\tilde{N}_1 \to \tilde{G}a_1 \to \tilde{G}b\bar{b}$. Although the last step in the decay chain always ensures the presence of b's in the final state, they are usually too soft to satisfy the requirements of current b-jet + p_T^{miss} searches. We find that b-jet searches only become sensitive when the mass of the gluino is high enough that decays into third generation squarks dominate and their decays into top/bottom quarks (see an example

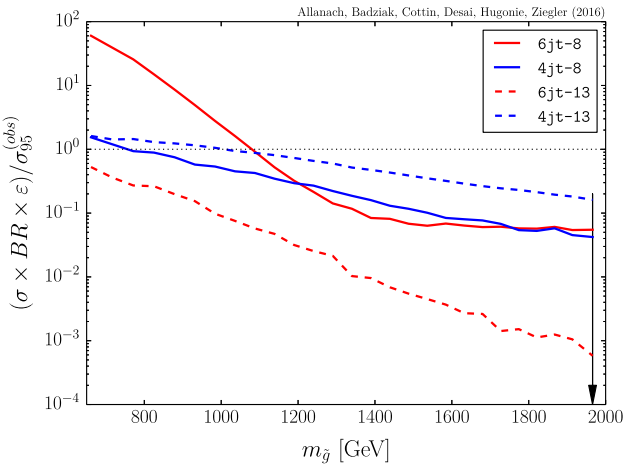

Fig. 3 95 % lower limits on the gluino mass from Run I and Run II jets + p_T^{miss} searches. We show the ratio of the predicted gluino cross section times branching ratio times acceptance ($\sigma \times BR \times \varepsilon$) to the 95 % upper bound on signal cross sections determined by ATLAS, for a scan-line based on benchmark P0 ($\tilde{N}_1$ lifetime of $c\tau_{\tilde{N}_1} = 99$ mm). The *horizontal dotted line* shows the exclusion limit at $r = (\sigma \times BR \times \varepsilon)/\sigma_{95}^{\text{obs}} = 1$. The *arrow* shows the position of our benchmark P0 in NMGMSB, whereas elsewhere we are strictly in pNMSSM parameter space

event topology in Fig. 1) result in high-p_T b-jets. Therefore these searches are never relevant for our benchmark P0 and the corresponding pNMSSM line that has even lower gluino masses. Note, however, that even when the gluino mass is high, the gluino branching fraction into b's is still only about 20 % and is often accompanied by vector bosons in the final state. These sometimes produce leptons, which take events out of the 0-lepton + multi-jets + p_T^{miss} selection. As a result of the above considerations, the sensitivity is much lower than that from simplified models producing hard b-jets and missing transverse momentum. We find that the sensitivity in the simplest 0-lepton + jets + p_T^{miss} searches is greater than that of searches involving bs even at high gluino masses. The signal regions (i.e. the labelled sets of cuts) defined by ATLAS that have the highest sensitivity are the `4jt-8` and `6jt-8` signal regions (relevant for 8 TeV collisions) and the `4jt-13` and `6jt-13` signal regions (relevant for 13 TeV collisions). We reproduce the cuts in these signal regions in Table 1 along with the observed upper limits on production cross section at the 95 % confidence level (CL).

Since in the DGS model the gluino sets the overall mass scale of the sparticle spectrum, we therefore present our results in the form of bounds on the gluino mass. We define the signal strength ratio r_{95} as the ratio of the predicted sparticle signal passing the selection cuts in a particular signal region to the 95 % CL upper limit on the cross section in that region. Thus $r_{95} = 1$ is *just* ruled out to 95 % CL, $r_{95} > 1$ is ruled out whereas $r_{95} < 1$ is allowed at the 95 % CL. The signal region is always chosen to be the one giving the best *expected* exclusion. Figure 3 shows the signal strength

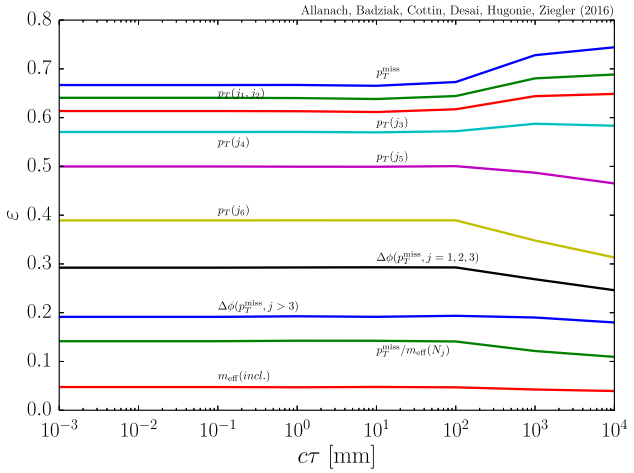

Fig. 4 The dependence of overall efficiency on lifetime in the signal region `6jt-8`. We find that the strong dependence on $p_T^{\rm miss}$ is strongly anti-correlated with the cuts on jet p_T, resulting in a fairly small dependence of the efficiency on $c\tau$ after all cuts. The curves correspond from top to bottom to the cuts in Table 1 and the corresponding variables are shown in the *plot*

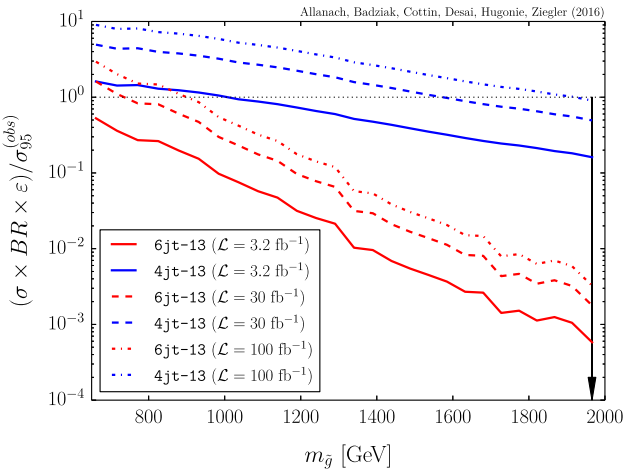

Fig. 5 95 % CL limits the gluino mass from the $\sqrt{s} = 13$ TeV jets + $p_T^{\rm miss}$ searches and projected sensitivity with higher luminosity in the pNMSSM model. The signal regions `4jt-13` and `6j-13` are defined in Table 1. The *arrow* shows the position of our benchmark P0 in NMGMSB, whereas elsewhere we are strictly in pNMSSM parameter space

ratio for varying gluino mass based on the pNMSSM line described in Sect. 3. The most sensitive signal region for gluinos from 0.9 to 1.2 TeV is the `6jt-8` region (six hard jets, tight cuts) at $\sqrt{s} = 8$ TeV. For higher gluino masses up to 2 TeV, the sensitivities of the `6jt-8` and `4jt-8` signal regions are similar. The presence of a long-lived singlino which may decay within the detector leads to another possible signature—that of DVs, which we shall explore in the next section. We see from the figure that the bound from Run I at 95 % is $m_{\tilde{g}} > 1080$ GeV, where the `6jt-8` line intersects $r_{95} = 1$.

In 2015, ATLAS analysed 3.2 fb^{-1} of integrated luminosity collected at the higher centre of mass energy of 13 TeV, not observing any significant signal for sparticle production. We see that at 13 TeV, the `4jt-13` cuts are more sensitive to our pNMSSM model than the `6jt-13` cuts for any value of the gluino mass, mainly because the p_T requirements are not satisfied by the jets from singlino decay products (which give $N_{\rm jets} > 4$). We see that the early Run II data from 2015 constrained $m_{\tilde{g}} > 1000$ GeV, not as sensitive as the Run I limit. Later, we shall examine the expected sensitivity from Run II with 100 fb^{-1} of integrated luminosity.

In Fig. 4, we show how changing the lifetime of the $\tilde{N}_1$ affects the cut acceptances (shown here for the signal region `6jt-8`). The lines should be read in one-to-one correspondence from top to bottom with the cuts listed in Table 1 (except the second line which is the combined efficiency for $p_T(j_1)$ and $p_T(j_2)$). Thus, the first line corresponds to the cut $p_T^{\rm miss} > 160$ GeV and the last to $m_{\rm eff} > 1500$ GeV. As expected, when the singlino is stable, we find large missing energy as all the momentum it carries is invisible. As the lifetime decreases, more and more singlinos decay within the detector volume resulting in a flat efficiency below lifetimes of 10 mm. This gain in efficiency for long-lived $\tilde{N}_1$ is somewhat diluted once we demand jets with high p_T. In particular, once we demand $N_{\rm jets} > 4$, the efficiency is lower for stable singlinos, since the extra hard jets mainly come from decay products of the $\tilde{N}_1$. However, this downturn is balanced by the requirements on $\Delta\phi$ between the jets and the missing momentum $p_T^{\rm miss}$, since the presence of more jets in the final state makes it harder to satisfy this cut. Finally, after all cuts, we find that the efficiency is rather flat across all lifetimes. Therefore the gluino mass limits presented above may be considered fairly robust for the model studied here.

3.2 Future search reach of prompt searches

We now estimate what the future might bring for discovery or exclusion of the pNMSSM model from the LHC. In Fig. 5, we re-display the current limits on the gluino in pNMSSM from the 13 TeV run, as the gluino mass is changed for the `6jt-13` and `4jt-13` signal regions. The solid lines show the current lower limit from the 2015 run of 1000 GeV. For our model, the `4jt-13` region performs better than the `6jt-13` region. Model sensitivity (ignoring systematic errors) is equal to the number of signals events S divided by the square root of the number of background events B. Since $S \propto$ the total integrated luminosity $\mathcal{L}$, and $B \propto \mathcal{L}$, the sensitivity scales $\propto \sqrt{\mathcal{L}}$. Thus, we expect $\sigma_{95}^{\rm obs} \propto 1/\sqrt{\mathcal{L}}$. Using this dependence, we scale the $\mathcal{L} = 3.2$ fb^{-1} lines to 30 and 100 fb^{-1} to show the projected sensitivities in the figure. We see that

with 100 fb^{-1} and 13 TeV centre of mass collision energy, the LHC can reach up to 1900 GeV gluinos.

4 Searches with displaced vertices

DV searches are especially challenging due to the complication of taking into account time of flight and assigning tracks originating far away from the primary interaction point to the correct event. Reconstruction of such decays therefore becomes more difficult beyond the pixel layers. Nevertheless, these searches have an extremely low background as there are no irreducible contributions from the SM. Some recent reinterpretation of LHC displaced searches can be found in Refs. [45–51]. Displaced signatures have received far less attention in the literature as compared to prompt signatures because they are difficult to model, and because they tend to be rather model specific. Furthermore, modelling the detector's response to DVs is a difficult task, as we shall illustrate. Validation is therefore essential in order to tell how good or bad a job of modelling the response we achieve. References [45,47] used truth information to identify displaced decays. Our work goes further by fully detailing the steps of reconstruction for DVs, in a similar way to Ref. [46], but here we determine an explicit functional form for the tracking efficiency, which is needed to be able to model the efficiencies from the experiments to a reasonable (if somewhat rough) level.

4.1 Validation of Run I displaced vertex searches

In the absence of publicly available multi-dimensional, model-independent efficiency maps for the reconstruction efficiency of a DV, we make use of the efficiencies published for specific models and construct a function that approximately simultaneously reproduces them. The ATLAS DV + jets search [52] has been interpreted in the context of two General Gauge Mediation (GGM) and several R-parity violating supersymmetry (RPV) simplified models. Of these, the ones most relevant to signatures predicted by the DGS model (where we expect only jets from the DV) are the two GGM model benchmarks and one RPV benchmark where a displaced neutralino decays through a non-zero λ'_{211} to light quarks and a muon.

The ATLAS DV + jets cuts are summarised in Table 2. The ATLAS analysis re-runs the experiment's standard tracking algorithms on events passing the trigger in order to determine the efficiency for the displaced tracks. Given the fact that we do not have access to such algorithms, we assign each track a reconstruction probability depending on its p_T and the *true* co-ordinates of its displaced origin. The functional form found to reproduce the efficiencies for the three benchmark models is given by

Table 2 Our implementation of cuts applied in the ATLAS multi-track DV + jets search, from Ref. [52]

DV jets	4 or 5 or 6 jets with $\|\eta\| < 2.8$ and $p_T > 90, 65, 55$ GeV, each
DV reconstruction	DV made from tracks with $p_T > 1$ GeV, $\|\eta\| < 2.5$ and $\|d_0\| > 2$ mm, satisfying a tracking efficiency given by Eq. 2. Vertices within 1 mm are merged
DV fiducial	DV within 4 mm $< r_{\mathrm{DV}} <$ 300 mm and $\|z_{\mathrm{DV}}\| <$ 300 mm
DV material	No DV in regions near beampipe or within pixel layers: Discard tracks with $r_{\mathrm{DV}}/\mathrm{mm} \in$ {[25, 38], [45, 60], [85, 95], [120, 130]}
N_{trk}	DV track multiplicity $\geq$5
m_{DV}	DV mass >10 GeV

$$\begin{aligned}\varepsilon_{\mathrm{trk}} &= 0.5 \times (1 - \exp(-p_T/[4.0\ \mathrm{GeV}])) \\ &\quad \times \exp(-|z|/[270\ \mathrm{mm}]) \\ &\quad \times \max(-0.0022 \times r_\perp/[1\ \mathrm{mm}] + 0.8, 0), \end{aligned} \tag{2}$$

where $r_\perp$ and z are the transverse and longitudinal distance of the track's production vertex (for details of their definitions, see Appendix A).

We pick this particular parameterisation of the tracking efficiency after trying several functional forms and varying the constants, picking the one that had the best goodness of fit statistic (χ^2) for the three models combined that we validate against (at various different values of lifetimes of the decaying sparticle). Equation (2) is not expected to be perfect by any stretch: it is a simple, universal and factorised form for the track efficiency that is a rough approximation. The overall χ^2 statistic did not indicate a particularly good fit; however, inspection by eye showed that the shapes of the efficiency curves were reasonable. We display contours of the function in Fig. 6.

The efficiency for reconstructing a multi-track DV is highly dependent on track reconstruction and track selection, as detailed in Ref. [52]. These are affected by several factors:

- The impact parameter d_0 of the track: the efficiency for reconstructing tracks decreases with increasing values of d_0, since the density of fine instrumentation decreases.
- The mass of the long-lived particle: as the number of tracks originating from the vertex increases with increasing mass. At higher masses, missing some tracks may therefore still lead to the identification of a DV.
- The energy of the long-lived particle: the higher the boost, the more tracks will have a small angle with respect to the flight direction of the long-lived particle and may therefore fail the minimal d_0 cut.

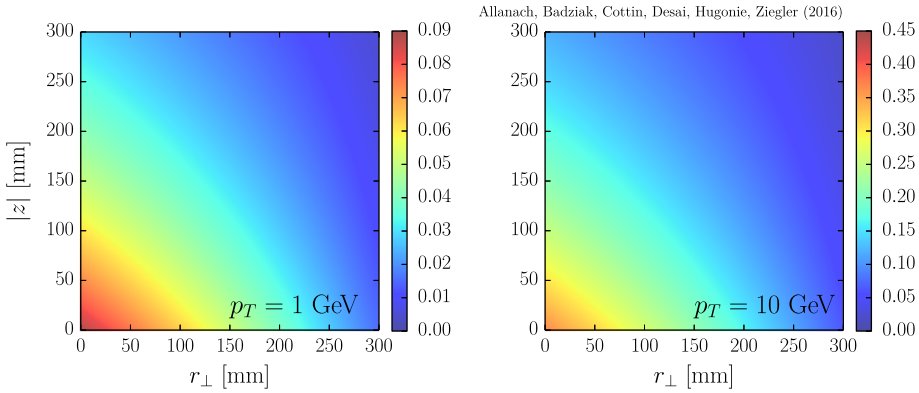

Fig. 6 Contours of track efficiency as a function of $r_\perp$ and $|z|$, for a p_T value fixed at 1 GeV (*left*) and 10 GeV (*right*). Note the difference scales of track efficiency (labelled by the legend at the *right-hand side*) of each panel

We can therefore see that the vertex reconstruction efficiency will be a non-trivial combination of different aspects of the track reconstruction efficiency. For instance the vertex reconstruction efficiency is worst at large radii, which is due to tracking efficiency decreasing. Here, we focus only on assigning each track a reconstruction probability dependent on some relevant variables, such as the transverse and longitudinal distance of the production vertex of the track and its transverse momentum. The particular choice of the variables in Eq. 2 (for instance the fact we use $r_\perp$ instead of d_0) was made because we found these fitted the best across the three different signal models out of a few different simple factorised functional forms that we tried.

We find that validating against only one of the benchmark models at a time leads to different best-fit parameters for each. Using three benchmarks for validation therefore gives us more confidence in applying the efficiency to our own model. We believe this is a key improvement in our work. Choosing a functional form for the tracking efficiency in order to recast displaced results has already been attempted in the literature [46]. Here we show the explicit functional form used, since knowing it is necessary to be able to reproduce our results. Figure 7 shows the validation of our simulation (dashed lines) for three different ATLAS benchmarks, against the ATLAS determination (solid lines). We see that the efficiency, while far from being perfectly modelled by our function, is adequately modelled (within a few sigma) for most of the range of lifetimes considered. We could improve the above fits by including an additional selection efficiency at the vertex level, as discussed above. We could also take into account the topology of the different signatures. Ideally, a parameterisation of the tracking efficiency should be validated against all the ∼20 signal benchmarks used in the ATLAS search, which is beyond the scope of this paper and which we leave for a future work.

Undiscarded displaced tracks are input into our vertex reconstruction algorithm, which compares and clusters the tracks' origins.[4] If the origins of two displaced tracks are less than 1 mm apart, then they are clustered together into one DV. Picking the first track, we compute the d value (i.e. the physical distance in the laboratory frame $\sqrt{\Delta x^2 + \Delta y^2 + \Delta z^2}$) to each of the other tracks, clustering tracks that have a small enough d value to the first track. Then we repeat for the next unclustered track and so on, until each track is assigned to a single vertex. The ATLAS analysis (and ours) combines vertices into a DV if they are less than $d = 1$ mm apart. The DV position is defined as the average position of all the track origins in the cluster.

To ensure consistency of the vertex position and the direction of the tracks, we require at least two tracks in the vertex to have $\mathbf{d} \cdot \mathbf{p} > -20$ mm, where we define $\mathbf{d}$ to be the vector from the interaction point to the DV and $\mathbf{p}$ to be the momentum of the displaced track. In the ATLAS analysis, DVs are vetoed if they are reconstructed in high density material regions, since this is the main source of background vertices. We simulate this by requiring 4 mm $< r <$ 300 mm and $|z| <$ 300 mm. We also require decay positions of the DVs to not be inside any of the three ATLAS pixel layers (our approximation to this DV material cut is shown in Table 2).[5] As the table shows, events are further selected if they have at least one reconstructed DV with five tracks or more and a DV invariant mass (computed assuming all tracks have the pion mass) of at least 10 GeV.

4.2 Run I sensitivity of displaced vertex searches

We now apply the simulation described in the previous section to the DGS model benchmark P0. We find that the sensitivity of the ATLAS study to our benchmark is extremely

[4] ATLAS performs a complicated vertex χ^2 fit in order to reconstruct DVs. Here, we simply use the truth information to define the track's origin to be the point at which the $\tilde{N}_1$ decays, and start comparing the distance between tracks' origins to cluster them into vertices.

[5] Note that the material veto performed in the ATLAS analysis is far more complex than this, since ATLAS makes use of a 3D material map of the detector that we do not have access to.

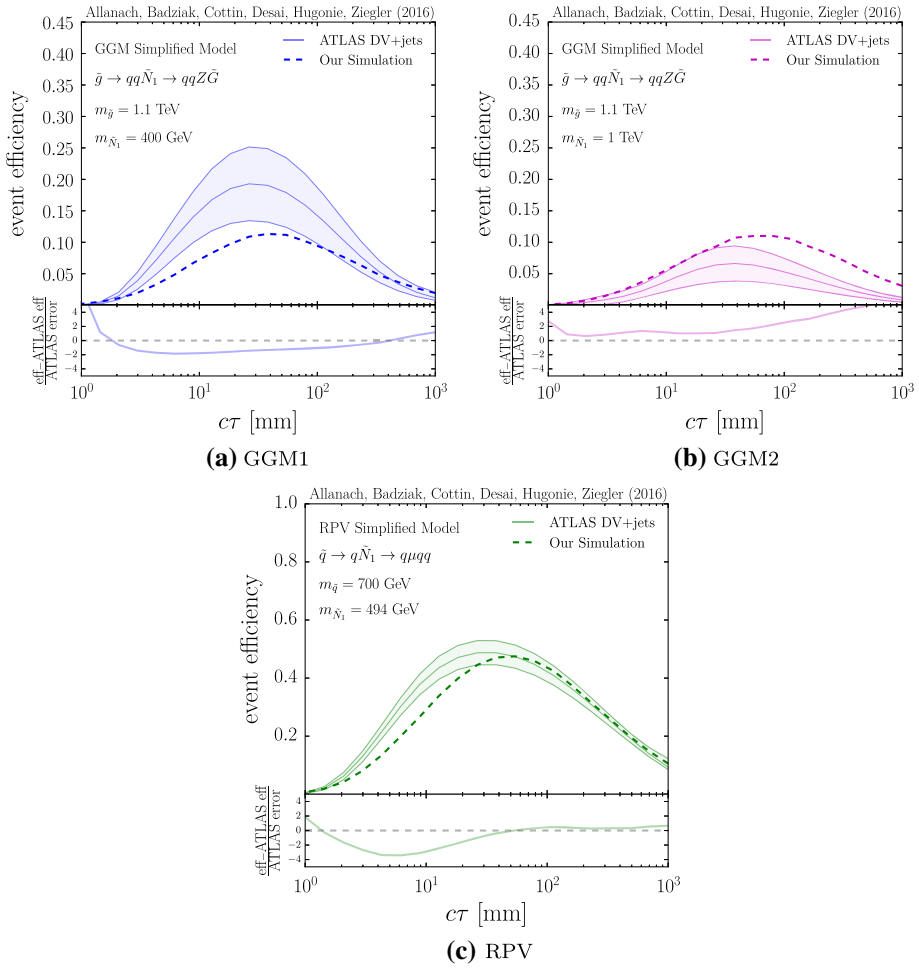

Fig. 7 Validation of our DV + jets estimate of efficiency for three models against ATLAS's determination: **a** a simplified GGM model where a 1.1 TeV gluino decays to a 400 GeV neutralino, which in turn decays to a Z and a gravitino, **b** a simplified GGM model where a 1.1 TeV gluino decays to a 1 TeV neutralino, which in turn decays to a Z and a gravitino, **c** a simplified RPV model with a 700 GeV squarks decaying to a 500 GeV neutralino, which subsequently decays through a non-zero λ'_{211} coupling into a muon and two quarks. Events are generated with $\sqrt{s} = 8$ TeV. The *bottom rectangle* in each case shows the discrepancy between our estimate and ATLAS's, measured in units of the ATLAS error

Table 3 Numbers of simulated events N and relative efficiencies ϵ (i.e. defined with respect to the previous cut) for our NMGMSB model (P0 benchmark) with $c\tau_{\tilde{N}_1} = 99$ mm at $\sqrt{s} = 8$ TeV and $\sqrt{s} = 13$ TeV for the ATLAS selection of cuts in Table 2

	$\sqrt{s} = 8$ TeV		$\sqrt{s} = 13$ TeV	
	N	ϵ (%)	N	ϵ (%)
All events	100,000	100.0	100,000	100.0
DV jets	96,963	97.0	98,306	98.3
DV reconstruction	16,542	17.1	16,542	16.8
DV fiducial	16,459	99.5	16,460	99.5
DV material	16,146	98.1	16,210	98.5
N_{trk}	584	3.6	544	3.4
m_{DV}	4	0.7	3	0.6

limited. From the 8 TeV columns of Table 3, it is clear that the primary cause for this is failure to satisfy the requirements $N_{\text{trk}} \geq 5$ and the vertex mass cut $m_{\text{DV}} > 10$ GeV. This is due to the fact that the displaced jets are mainly b-jets. The b-hadrons are themselves long-lived, and the neutral B^0 leaves no tracks before its decay. The topology of this final state then has two further DVs, each with less than five tracks. The ATLAS analysis does merge vertices (defined as having at least two tracks) that are within 1 mm of each other to possibly obtain a better vertex. However, the b-hadrons are sufficiently long-lived so that the resultant vertices are almost always more than 1 mm apart.[6] For the benchmark P0 for instance, the average displaced track efficiency is 0.06, and the average number of tracks coming from a displaced b is 18.1 (after hadronisation, but before cuts). Thus, on average, there are only $18.1 \times 0.06 = 1.2$ visible tracks per displaced b.

A further consideration is the small mass of the a_1 which decays to $b\bar{b}$ (23 GeV for the benchmark P0) since softer b-quarks means less radiation, implying fewer tracks. The distribution of track multiplicity versus invariant mass is shown in Fig. 8. One can see clearly from the right panel that increasing the a_1 mass to 70 GeV (done ad hoc for the purposes of

[6] The ATLAS analysis [52] also reports that the sensitivity is severely reduced if they use the RPV benchmark with b-quarks in the final state. An earlier work on displaced Higgs decays [48], also shows how displaced b-quarks can be problematic, particularly given the $d < 1$ mm requirement for merging vertices.

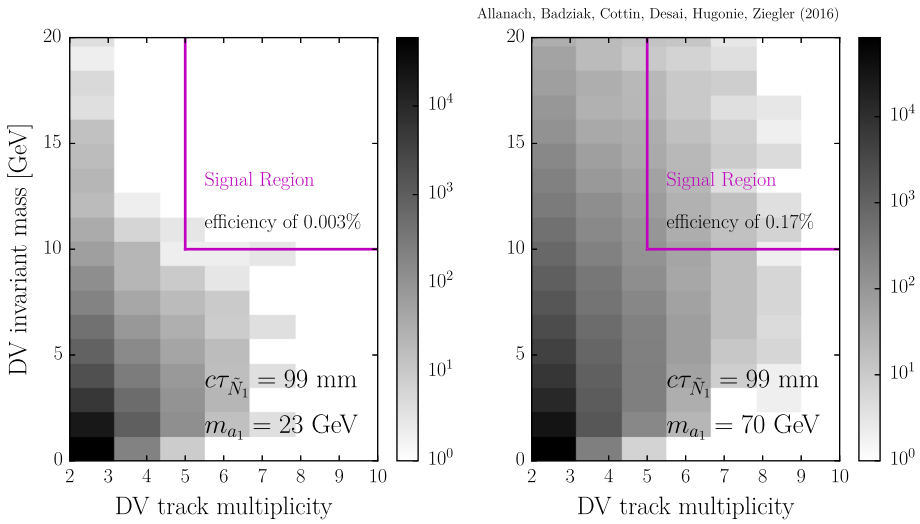

Fig. 8 DV invariant mass against number of tracks for the DGS benchmark P0 with $m_{\tilde{g}} = 1.96$ TeV, $m_{\tilde{N}_1} = 98$ GeV and $c\tau_{\tilde{N}_1} = 99$ mm. Gluinos and squarks only are generated with $\sqrt{s} = 8$ TeV. Events in the plot pass all of the DV cuts except for the last two, which define the boxed ATLAS signal region. The *left-hand frame* shows a scenario where $m_{a_1} = 23$ GeV (in the DGS good-fit region, as in P0) and the *right-hand frame* has a tweaked $m_{a_1} = 70$ GeV in the SLHA file (i.e. inconsistent with the soft parameters, which are left constant—for the purposes of illustration only)

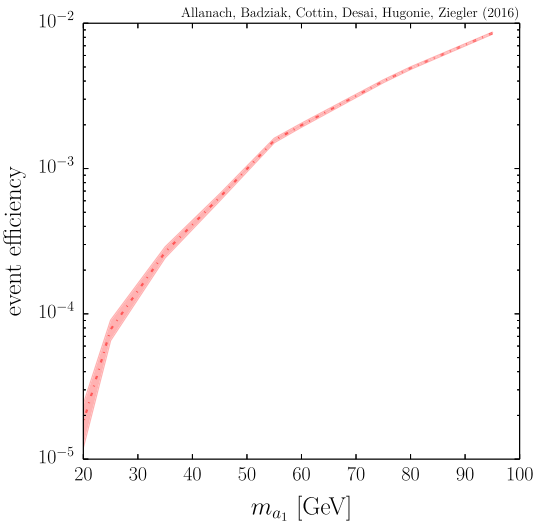

Fig. 9 Event efficiency against pseudo-scalar mass for a DGS benchmark with $c\tau_{\tilde{N}_1} = 99$ mm (our P0 benchmark). Events are generated with $\sqrt{s} = 8$ TeV considering strong production. We have tweaked m_{a_1} "by hand" in the SLHA files without changing soft parameters for the purposes of illustration

illustration) improves the sensitivity of the cuts by two orders of magnitude. A higher mass also means the resultant products are more collimated and hence the b-hadron vertices are likely to be closer to each other. The improvement in efficiency with increasing a_1 mass can be seen in Fig. 9.

4.3 Improving the sensitivity of displaced vertex searches

Given the very low sensitivity of the DV searches, we shall now attempt to improve it by loosening the most restrictive cuts. Firstly, to catch DVs coming from two b-quarks from the same a_1, we relax the requirement of maximum merging distance from 1 to 5 mm. Further, we can also relax the last two cuts: track multiplicity and invariant mass of the DV.

The background to the DV multi-track search comes from three sources—heavy flavour quark decays, interactions with material in the detector and the accidental crossing of tracks, all of which have a low multiplicity of tracks and a small invariant mass of the DV. Thus, if we loosen these cuts to achieve better signal efficiency, we also raise the background rate thus reducing the signal to background ratio. However, given that our model has good sensitivity in the prompt p_T^{miss}-based channels, background rates can be controlled by taking advantage of the hard prompt signals that come in association with the DVs. Requiring a large m_{eff} in the event would reduce backgrounds significantly. It may also be possible to increase the sensitivity by loosening the DV cuts but requiring displaced jets to have a muon inside them [53,54] (which often come from a b). However, we do not consider this route here.

We now investigate the effect of applying prompt cuts used in standard jets + p_T^{miss} sparticle searches on top of relaxed DV cuts. This, of course, will have a lower signal efficiency than purely applying the standard jets + p_T^{miss} cuts, which are already designed to remove the SM background very effectively. Ideally, one would optimise the jets + p_T^{miss} cuts along with the DV cuts to reach an overall best sensitivity. However, we have clear estimates of the background to the prompt channels from the analysis which serves as an upper bound to any DV contributions we may have from heavy flavour. Of course, the contributions from systematic sources cannot be bounded in this way, however, we can reasonably assume that the number of DVs from systematic sources is not biased by the hard cuts we place.

At 8 TeV, we choose the ATLAS `6jt-8` signal region cuts described in Table 1, because they were found to have the highest sensitivity to our signal, as shown above. Figure 10

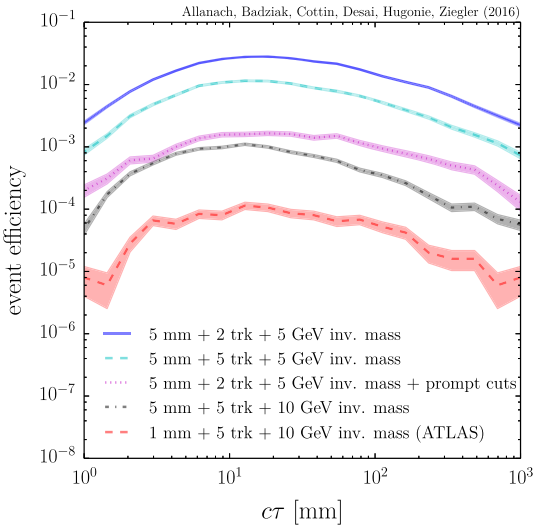

Fig. 10 Signal efficiencies of different sets of DV + jets analyses on a DGS benchmark with $m_{\tilde{g}} = 1.96$ TeV, $m_{\tilde{N}_1} = 98$ GeV, $m_{a_1} = 23$ GeV (our P0 benchamark) against the lifetime of the long-lived singlino $c\tau_{\tilde{N}_1}$ (changed "by hand" in the SLHA files without changing the soft terms for the purposes of illustration). Events are generated with $\sqrt{s} =$ 8 TeV, considering gluino/squark production only. The *bottom curve* corresponds to the efficiency after the default ATLAS DV cuts. The *top curve* corresponds to the loosest of our selections in DV merging distance, track multiplicity and invariant mass. We also show different sets of cuts in between, including the inclusion of standard prompt cuts, as defined in the text

Table 4 Numbers of simulated events N and relative efficiencies ϵ (i.e. defined with respect to the previous cut) for our NMGMSB model with $c\tau_{\tilde{N}_1} = 99$ mm (our P0 benchmark) at $\sqrt{s} = 8$ TeV and $\sqrt{s} =$ 13 TeV for our tuned cuts, as explained in the text. Events are generated considering strong production. An asterisk denotes that the prompt cuts are taken from signal regions `6jt-8` at $\sqrt{s} = 8$ TeV and `4jt-13` at $\sqrt{s} = 13$ TeV as listed in Table 1. The dagger is a reminder of the increased vertex merging distance of 5 mm

	$\sqrt{s} = 8$ TeV		$\sqrt{s} = 13$ TeV	
	N	ϵ (%)	N	ϵ (%)
All events	100,000	100.0	100,000	100.0
Prompt p_T^{miss}*	91,709	91.7	87,737	87.7
Prompt jets*	72,075	78.6	84,178	95.9
Prompt $\Delta\phi(\text{jet}_{1,2,3}, \mathbf{p}_T^{\text{miss}})_{\text{min}}$*	49,095	68.1	57,261	68.0
Prompt $\Delta\phi(\text{jet}_{j>3}, \mathbf{p}_T^{\text{miss}})_{\text{min}}$*	27,315	55.6	33,832	59.1
Prompt $p_T^{\text{miss}}/m_{\text{eff}}(N_j)$*	6670	24.4	18,409	54.4
Prompt m_{eff}(incl.)*	6636	99.5	16,848	91.5
DV jets	6636	100.0	16,848	100.0
DV reconstruction†	1524	23.0	3850	22.9
DV fiducial	1516	99.5	3825	99.4
DV material	1494	98.5	3750	98.0
$N_{\text{trk}} \geq 2$	1494	100.0	3750	100.0
$m_{\text{DV}} > 5$ GeV	88	5.9	265	7.1

shows efficiency curves against lifetime for the NMGMSB model with the default ATLAS DV analysis cuts and some choices of relaxed cuts. This includes (1) allowing N_{trk} to be ≥ 2 rather than ≥ 5, (2) increasing the vertex merging distance from 1 to 5 mm, and (3) lowering the vertex mass cut from 10 to 5 GeV. For comparison, we also show the response for the original tight ATLAS DV (`DVT`) cuts as well as our loose cuts (`DVL`) for the `6jt-8` signal region. With this combination, we already achieve an improvement in signal efficiency by a factor of ten. Without the `6jt-8` cuts, the improvement is a factor of several hundred. An optimised analysis will be between these two limiting cases and may therefore be reasonably expected to offer an improvement of two orders of magnitude or so.

4.4 Recommendations for displaced vertex searches at 13 TeV

We used `6jt-8` for the prompt cuts at 8 TeV; however, keeping in mind that the best sensitivity at 13 TeV is for the `4jt-13` signal region, we also perform efficiency calculations with the combination `DVL + 4jt-13`. The efficiencies are shown in Table 4. The signal efficiency at 13 TeV is ∼0.2 %. It would be desirable to relax the prompt cuts further in order to increase this number, but a proper estimate would require a full estimation of the DV background, which is beyond the scope of this paper.

However, an estimate of the contribution from heavy flavours may be obtained. Given the hard multi-jet, p_T^{miss} and m_{eff} cuts, the dominant SM background is from $t\bar{t}$ + jets production which is also a source of b-hadrons and therefore a potential background for DVs. In order to examine this possibility, we simulate 10^6 $t\bar{t}$ events, and inspect the transverse impact parameter d_0 of the tracks coming from the displaced b vertices. We see that only a tiny fraction of tracks pass $|d_0| > 2$ mm from $t\bar{t}$ events (∼1 %). Furthermore, imposing the DV cuts (without any restrictions on hard jets), gives us an efficiency of 0.1 % for $N_{\text{trk}} \geq 2$ and imposing $m_{\text{DV}} > 5$ GeV gives us no events at all. We therefore do not expect any DV contributions from heavy flavour once the hard jet cuts are made. This implies zero background events at 3.2 fb^{-1} and we are already potentially sensitive to signal cross sections of approximately 0.3 fb.

The total strong sparticle production cross section at 13 TeV before cuts is 5.8 fb, and so with our illustrative cuts (`DVL + 4jt-13`), one would achieve a signal cross section after cuts of 0.01 fb. With no expected background, the observation of a single event already corresponds to discovery, which for a gluino mass of ∼2 TeV (as in P0) is not achievable in prompt search channels with 100 fb^{-1} at 13 TeV. We may reasonably set the observation of at least

three signal events as a requirement for discovery, which results in a best-case scenario of discovering a NMGMSB model with $m_{\tilde{g}} \sim 2$ TeV with 300 fb^{-1} data at 13 TeV.

We can also make an estimate of the worst-case scenario where there is a large DV background from systematic sources. Such a background occurs when a spurious track crosses an existing DV resulting in a reconstructed vertex satisfying the $N_{\rm trk}$ and $m_{\rm DV}$ requirements. The ATLAS DV analysis [52] estimates only ∼0.4 background vertices in the DV + jet channel for the full 20 fb^{-1} data of Run I (see Table 1 of Ref. [52]). Given a $t\bar{t}$ production cross section $\sim O(100$ pb) at 8 TeV, this implies an efficiency $\sim 10^{-5}$. To be conservative about the effect of our relaxed cuts, we can assume that this happens in about 1 % of events that pass the `4jt-13` cuts. Starting with a total prompt background of ∼1 fb (see Table 4 of Ref. [44]) in the `4jt-13` channel as reported in the ATLAS analysis, we arrive at 0.01 fb for `DVL` + `4jt-13`. A 3-sigma discovery may then be viable with ∼1 ab^{-1} data at 13 TeV.

This situation may be improved considerably by relaxing the prompt cuts. An indication of where we may further relax the selection cuts comes from examining the relative efficiencies at 8 and 13 TeV for the cut on the ratio of $p_T^{\rm miss}$ and $m_{\rm eff}(N_j)$. We see that a change from >0.25 at 8 TeV to >0.2 at 13 TeV (see Table 1) already results in a gain of a factor 2. Although this is obviously also due to the increased energy of the overall event, given that we have high $p_T^{\rm miss}$ and $m_{\rm eff}$ cuts, an additional factor of 3 may be gained by dropping the $p_T^{\rm miss}/m_{\rm eff}(N_j)$ cut altogether.

We now study how the cut efficiencies behave with singlino lifetime for benchmark P0. The result is shown in Fig. 11, where we plot the effect of the cuts `DVL` + `4jt-13` as a function of the decay length $c\tau_{\tilde{N}_1}$. Note that we have merged the $m_{\rm eff}$(incl.) and the DV jets cuts together into one curve, as applying the DV jets cut after the $m_{\rm eff}$(incl.) one does not change the number of events, for any lifetime (this can also be appreciated for P0 in Table 4). We notice that standard prompt cuts are not very much affected by the singlino lifetime, except for the cut on the ratio of $p_T^{\rm miss}$ and $m_{\rm eff}(N_j)$, which increases at higher lifetimes. This is because $p_T^{\rm miss}$ is higher at high lifetimes, as explained in Sect. 3.1.

To summarise, with a combination of relaxed DV cuts and prompt SUSY search cuts, one can discover a NMGMSB scenario with $m_{\tilde{g}} \sim 2$ TeV with 300 fb^{-1} data which is not possible with prompt SUSY searches alone. With a full optimisation of relaxed DV cuts + prompt $p_T^{\rm miss}$-based cuts, we may easily gain a further factor of ten in the signal efficiency and given almost zero background, as shown above, one could have higher sensitivity to the NMGMSB model in DV + prompt searches as compared to prompt searches. We therefore strongly urge the experiments to perform a dedicated background simulation with optimised cuts.

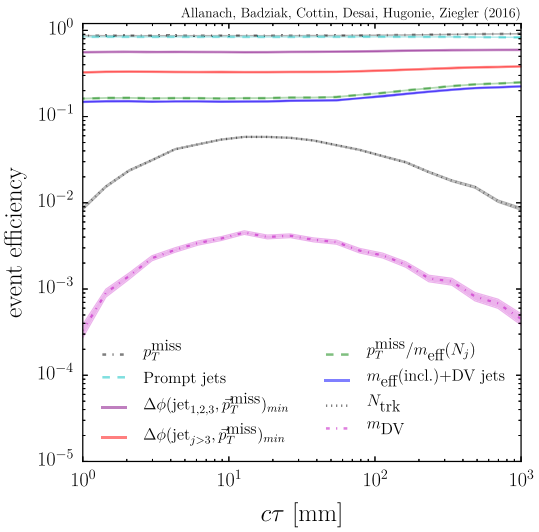

Fig. 11 Signal event efficiency of our simulation on a DGS benchmark with $m_{\tilde{g}} = 1.96$ TeV, $m_{\tilde{N}_1} = 98$ GeV, $m_{a_1} = 23$ GeV (our P0 benchmark) against the lifetime of the long-lived singlino $c\tau_{\tilde{N}_1}$. Events are generated with $\sqrt{s} = 13$ TeV considering strong production. Independent prompt and DV cuts are presented. The singlino decay distance $c\tau$ has been tweaked "by hand" in the SLHA files without changing soft parameters for the purposes of illustration

5 Summary

We have examined the prospects for discovery or exclusion of the DGS-NMGMSB model. The model has some nice properties: the SUSY flavour problem is addressed by gauge-mediated SUSY breaking, while the Higgs mass is made heavy enough through the mixing with the NMSSM CP-even singlet. This singlet has a mass around 90 GeV, and therefore can be made consistent with some small excesses in the LEP Higgs searches. An interesting feature of the model is the presence of a gravitino LSP and a singlino-like neutralino NLSP that can be long-lived.

As well as having the usual hard jets plus missing transverse momentum signatures, the model predicts possible DVs from long-lived singlinos. These decay into $b\bar{b}$ and missing transverse momentum in the form of gravitinos. However, displaced b's are somewhat problematic since B mesons themselves travel a small distance before visibly decaying and the 'displaced displaced' vertices have a very poor signal efficiency for getting past the standard DV cuts. We have illustrated how loosening the DV searches whilst imposing some prompt cuts to control background results in significantly higher signal efficiency, motivating a proper study with a full detector simulation (DV analyses are difficult to perform accurately from outside the experimental collaborations). We have provided a rough approximation to the tracking efficiency that works for two General Gauge Mediation models and one R-parity violating model over a range of

possible DV lifetimes, but clearly more work can be done to provide a more comprehensive parameterisation.

We have recast current 8 TeV prompt searches to bound the gluino mass from below at 1080 GeV, whereas current 13 TeV prompt searches are less restrictive. This is somewhat low compared to naive expectations based on LHC exclusion results quoted for simplified models, but as Fig. 2 shows, there are many different cascade decays in the model. This means that the supersymmetric signal ends up being shared out between many different channels, and may not be yet detected in any single one [3,4]. With 100 fb^{-1} of integrated luminosity at 13 TeV though, the 0-lepton + jets + p_T^{miss} searches should be sensitive to up to 1900 GeV.

We further combine the search strategies in the prompt and displaced channels to demonstrate that a much better sensitivity could be obtained by optimising cuts. In particular, we find that combining the relaxed DV cuts with the hard cuts from the 0-lepton + jets + p_T^{miss} analysis, a $>3\sigma$ discovery can be made with 300–1000 fb^{-1} data for a 2 TeV gluino mass depending on the systematic background. We indicate how this situation could be improved significantly by also relaxing some of the prompt cuts. It is clear that an optimised analysis in a DV + jets + p_T^{miss} channel will yield better sensitivity than for either search method alone and we strongly urge the experimental collaborations to pursue this further.

Acknowledgments The authors acknowledge the support of France Grilles for providing cloud computing resources on the French National Grid Infrastructure. This work has been partially supported by STFC Grant ST/L000385/1, by the Office of High Energy Physics of the U.S. Department of Energy under Contract DE-AC02-05CH11231, by the National Science Foundation under Grant PHY-1316783, by the Foundation for Polish Science through its programme HOMING PLUS, by National Science Centre under research Grant DEC-2014/15/B/ST2/02157, by the ILP LABEX under reference ANR-10-LABX-63, and by French state funds managed by the ANR within the Investissements d'Avenir programme under reference ANR-11-IDEX-0004-02. GC was funded by the postgraduate Conicyt-Chile Cambridge Scholarship 84130011. ND was partially supported by the Alexander von Humboldt Foundation. MB acknowledges support from the Polish Ministry of Science and Higher Education (Decision No. 1266/MOB/IV/2015/0). BCA, MB and GC would like to thank other members of the Cambridge SUSY Working group for discussions. RZ thanks B. Fuks, A. Mariotti, D. Redigolo and O. Slone for useful discussions. We thank the authors of `Delphes3` for discussions about the program related to this work. ND and MB would like to thank the Cavendish Laboratory for hospitality offered while working on this project. MB and RZ thanks the Galileo Galilei Institute for Theoretical Physics and INFN for hospitality and partial support during the completion of this work.

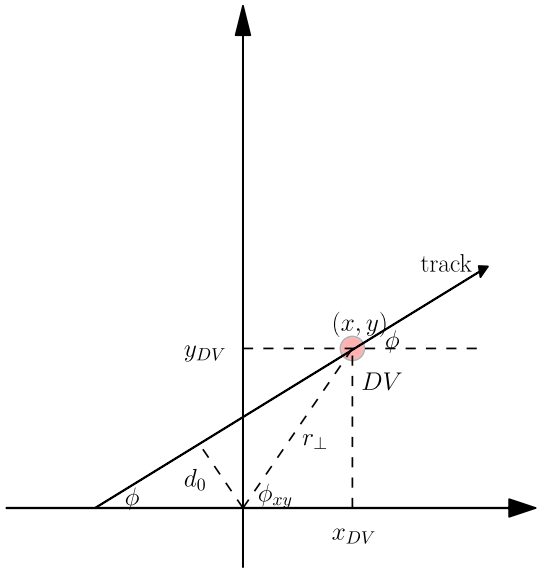

Fig. 12 Schematic view in the transverse x–y plane of a displaced decay. The transverse impact parameter d_0 is defined with respect to the origin $(0, 0, 0)$. The daughter particle, which forms the track, was produced at (x, y, z) from the decay of a long-lived particle. The DV position is reconstructed from the average of all track's production vertices, represented by the *pink* disc

Appendix A: Definitions of displaced observables

Here we define the relevant observables used in the DV recast. When a displaced track is produced at a point[7] (x, y, z), we define the transverse distance of the truth track's production vertex to be

$$r_\perp = \sqrt{x^2 + y^2}. \tag{A.1}$$

Each track will have a transverse impact parameter d_0, which corresponds to the distance of closest approach of the track to the origin $(0, 0, 0)$ in the x–y plane:

$$d_0 = r_\perp \times \sin(\phi_{xy} - \phi), \tag{A.2}$$

where ϕ is the azimuthal angle of the track, such that $\tan\phi = p_y/p_x$ with p_x, p_y the x and y component of the track momentum. ϕ_{xy} corresponds to the angle in the transverse plane of the trajectory of the mother displaced particle, as shown in Fig. 12.

Selected tracks are clustered together to form a DV. The DV position $(x_{\text{DV}}, y_{\text{DV}}, z_{\text{DV}})$ is defined to be the average position of all track's production points in that selected vertex. The DV position in the transverse plane is defined to be

$$r_{\text{DV}} = \sqrt{x_{\text{DV}}^2 + y_{\text{DV}}^2}. \tag{A.3}$$

[7] The origin is defined to be the interaction point, and z is along the beam line.

The DV position (x_{DV}, y_{DV}, z_{DV}) is equal to the truth decay position of the mother particle in principle, but in our simulation it is defined from the displaced tracks, using the truth information for the production positions, as explained above.

References

1. G. Aad et al., JHEP **10**, 054 (2015). doi:10.1007/JHEP10(2015)054
2. L.J. Hall, D. Pinner, J.T. Ruderman, JHEP **04**, 131 (2012). doi:10.1007/JHEP04(2012)131
3. G. Aad et al., JHEP **10**, 134 (2015). doi:10.1007/JHEP10(2015)134
4. A. Barr, J. Liu, arXiv:1605.09502 (2016)
5. J.L. Evans, M. Ibe, T.T. Yanagida, Phys. Lett. B **705**, 342 (2011). doi:10.1016/j.physletb.2011.10.031
6. T. Jelinski, J. Pawelczyk, K. Turzynski, Phys. Lett. B **711**, 307 (2012). doi:10.1016/j.physletb.2012.04.011
7. J.L. Evans, M. Ibe, S. Shirai, T.T. Yanagida, Phys. Rev. D **85**, 095004 (2012). doi:10.1103/PhysRevD.85.095004
8. Z. Kang, T. Li, T. Liu, C. Tong, J.M. Yang, Phys. Rev. D **86**, 095020 (2012). doi:10.1103/PhysRevD.86.095020
9. N. Craig, S. Knapen, D. Shih, Y. Zhao, JHEP **03**, 154 (2013). doi:10.1007/JHEP03(2013)154
10. M. Abdullah, I. Galon, Y. Shadmi, Y. Shirman, JHEP **1306**, 057 (2013). doi:10.1007/JHEP06(2013)057
11. H.D. Kim, D.Y. Mo, M.S. Seo, Eur. Phys. J. C **73**(6), 2449 (2013). doi:10.1140/epjc/s10052-013-2449-z
12. P. Byakti, T.S. Ray, JHEP **1305**, 055 (2013). doi:10.1007/JHEP05(2013)055
13. N. Craig, S. Knapen, D. Shih, JHEP **08**, 118 (2013). doi:10.1007/JHEP08(2013)118
14. J.A. Evans, D. Shih, JHEP **1308**, 093 (2013). doi:10.1007/JHEP08(2013)093
15. L. Calibbi, P. Paradisi, R. Ziegler, JHEP **1306**, 052 (2013). doi:10.1007/JHEP06(2013)052
16. T. Jelinski, JHEP **1309**, 107 (2013). doi:10.1007/JHEP09(2013)107
17. I. Galon, G. Perez, Y. Shadmi, JHEP **1309**, 117 (2013). doi:10.1007/JHEP09(2013)117
18. W. Fischler, W. Tangarife, JHEP **1405**, 151 (2014). doi:10.1007/JHEP05(2014)151
19. S. Knapen, D. Shih, JHEP **1408**, 136 (2014). doi:10.1007/JHEP08(2014)136
20. R. Ding, T. Li, F. Staub, B. Zhu, JHEP **1403**, 130 (2014). doi:10.1007/JHEP03(2014)130
21. L. Calibbi, P. Paradisi, R. Ziegler, Eur. Phys. J. C **74**(12), 3211 (2014). doi:10.1140/epjc/s10052-014-3211-x
22. A. Basirnia, D. Egana-Ugrinovic, S. Knapen, D. Shih, JHEP **06**, 144 (2015). doi:10.1007/JHEP06(2015)144
23. T. Jelinski, PoS **CORFU2014**, 089 (2015)
24. T. Jelinski, J. Gluza, Phys. Lett. B **751**, 541 (2015). doi:10.1016/j.physletb.2015.11.003
25. S. Knapen, D. Redigolo, D. Shih, JHEP **03**, 046 (2016). doi:10.1007/JHEP03(2016)046
26. B. Allanach, M. Badziak, C. Hugonie, R. Ziegler, Phys. Rev. D **92**(1), 015006 (2015). doi:10.1103/PhysRevD.92.015006
27. A. Delgado, G.F. Giudice, P. Slavich, Phys. Lett. B **653**, 424 (2007). doi:10.1016/j.physletb.2007.07.057
28. G.F. Giudice, R. Rattazzi, Nucl. Phys. B **511**, 25 (1998). doi:10.1016/S0550-3213(97)00647-0
29. M. Badziak, M. Olechowski, S. Pokorski, JHEP **06**, 043 (2013). doi:10.1007/JHEP06(2013)043
30. S. Schael et al., Eur. Phys. J. C **47**, 547 (2006). doi:10.1140/epjc/s2006-02569-7
31. M. Badziak, I. Dalianis, Z. Lalak, JHEP **02**, 173 (2016). doi:10.1007/JHEP02(2016)173
32. U. Ellwanger, C. Hugonie, Comput. Phys. Commun. **175**, 290 (2006). doi:10.1016/j.cpc.2006.04.004
33. U. Ellwanger, C. Hugonie, Comput. Phys. Commun. **177**, 399 (2007). doi:10.1016/j.cpc.2007.05.001
34. A. Buckley, Eur. Phys. J. C **75**(10), 467 (2015). doi:10.1140/epjc/s10052-015-3638-8
35. T. Sjöstrand, S. Ask, J.R. Christiansen, R. Corke, N. Desai, P. Ilten, S. Mrenna, S. Prestel, C.O. Rasmussen, P.Z. Skands, Comput. Phys. Commun. **191**, 159 (2015). doi:10.1016/j.cpc.2015.01.024
36. M. Cacciari, G.P. Salam, G. Soyez, Eur. Phys. J. C **72**, 1896 (2012). doi:10.1140/epjc/s10052-012-1896-2
37. B.C. Allanach, Comput. Phys. Commun. **143**, 305 (2002). doi:10.1016/S0010-4655(01)00460-X
38. B.C. Allanach, P. Athron, L.C. Tunstall, A. Voigt, A.G. Williams, Comput. Phys. Commun. **185**, 2322 (2014). doi:10.1016/j.cpc.2014.04.015
39. M. Muhlleitner, A. Djouadi, Y. Mambrini, Comput. Phys. Commun. **168**, 46 (2005). doi:10.1016/j.cpc.2005.01.012
40. P.Z. Skands et al., JHEP **07**, 036 (2004). doi:10.1088/1126-6708/2004/07/036
41. B.C. Allanach et al., Comput. Phys. Commun. **180**, 8 (2009). doi:10.1016/j.cpc.2008.08.004
42. ATLAS Collaboration, G. Aad et al., arXiv:0901.0512 (2009)
43. G. Aad et al., JHEP **09**, 176 (2014). doi:10.1007/JHEP09(2014)176
44. ATLAS Collaboration, M. Aaboud et al., arXiv:1605.03814 (2016)
45. Z. Liu, B. Tweedie, JHEP **06**, 042 (2015). doi:10.1007/JHEP06(2015)042
46. C. Csaki, E. Kuflik, S. Lombardo, O. Slone, T. Volansky, JHEP **08**, 016 (2015). doi:10.1007/JHEP08(2015)016
47. Y. Cui, B. Shuve, JHEP **02**, 049 (2015). doi:10.1007/JHEP02(2015)049
48. C. Csaki, E. Kuflik, S. Lombardo, O. Slone, Phys. Rev. D **92**(7), 073008 (2015). doi:10.1103/PhysRevD.92.073008
49. J.A. Evans, J. Shelton, JHEP **04**, 056 (2016). doi:10.1007/JHEP04(2016)056
50. A. Coccaro, D. Curtin, H. J. Lubatti, H. Russell, J. Shelton, arXiv:1605.02742 (2016)
51. A. de la Puente, A. Szynkman, Eur. Phys. J. C **76**(3), 124 (2016). doi:10.1140/epjc/s10052-016-3969-0
52. G. Aad et al., Phys. Rev. D **92**(7), 072004 (2015). doi:10.1103/PhysRevD.92.072004
53. V.M. Abazov et al., Phys. Rev. Lett. **103**, 071801 (2009). doi:10.1103/PhysRevLett.103.071801
54. G. Aad et al., JINST **8**, P07015 (2013). doi:10.1088/1748-0221/8/07/P07015